Charged-pion cross sections and double-helicity asymmetries in polarized p+p collisions at sqrt[s]=200 GeV

A. Adare *et al.* (PHENIX Collaboration)

Phys. Rev. D **91**, 032001 — Published 2 February 2015

DOI: 10.1103/PhysRevD.91.032001

Charged-pion cross sections and double-helicity asymmetries in polarized p+p collisions at $\sqrt{s}$=200 GeV

A. Adare,[13] C. Aidala,[37,42] N.N. Ajitanand,[59] Y. Akiba,[55,56] R. Akimoto,[12] H. Al-Ta'ani,[49] J. Alexander,[59] K.R. Andrews,[1] A. Angerami,[14] K. Aoki,[55] N. Apadula,[60] E. Appelt,[64] Y. Aramaki,[12,55] R. Armendariz,[8] E.C. Aschenauer,[7] E.T. Atomssa,[60] T.C. Awes,[51] B. Azmoun,[7] V. Babintsev,[23] M. Bai,[6] B. Bannier,[60] K.N. Barish,[8] B. Bassalleck,[48] A.T. Basye,[1] S. Bathe,[5,56] V. Baublis,[54] C. Baumann,[43] A. Bazilevsky,[7] R. Belmont,[42,64] J. Ben-Benjamin,[44] R. Bennett,[60] D.S. Blau,[32] J.S. Bok,[67] K. Boyle,[56] M.L. Brooks,[37] D. Broxmeyer,[44] H. Buesching,[7] V. Bumazhnov,[23] G. Bunce,[7,56] S. Butsyk,[37] S. Campbell,[60] P. Castera,[60] C.-H. Chen,[60] C.Y. Chi,[14] M. Chiu,[7] I.J. Choi,[24,67] J.B. Choi,[10] R.K. Choudhury,[4] P. Christiansen,[39] T. Chujo,[63] O. Chvala,[8] V. Cianciolo,[51] Z. Citron,[60] B.A. Cole,[14] Z. Conesa del Valle,[34] M. Connors,[60] M. Csanád,[17] T. Csörgő,[66] S. Dairaku,[33,55] A. Datta,[41] G. David,[7] M.K. Dayananda,[20] A. Denisov,[23] A. Deshpande,[56,60] E.J. Desmond,[7] K.V. Dharmawardane,[49] O. Dietzsch,[58] A. Dion,[27,60] M. Donadelli,[58] O. Drapier,[34] A. Drees,[60] K.A. Drees,[6] J.M. Durham,[37,60] A. Durum,[23] L. D'Orazio,[40] Y.V. Efremenko,[51] T. Engelmore,[14] A. Enokizono,[51] H. En'yo,[55,56] S. Esumi,[63] B. Fadem,[44] D.E. Fields,[48] M. Finger,[9] M. Finger, Jr.,[9] F. Fleuret,[34] S.L. Fokin,[32] J.E. Frantz,[50] A. Franz,[7] A.D. Frawley,[19] Y. Fukao,[55] T. Fusayasu,[46] C. Gal,[60] I. Garishvili,[61] F. Giordano,[24] A. Glenn,[36] X. Gong,[59] M. Gonin,[34] Y. Goto,[55,56] R. Granier de Cassagnac,[34] N. Grau,[2,14] S.V. Greene,[64] M. Grosse Perdekamp,[24] T. Gunji,[12] L. Guo,[37] H.-Å. Gustafsson,[39,*] J.S. Haggerty,[7] K.I. Hahn,[18] H. Hamagaki,[12] J. Hamblen,[61] R. Han,[53] J. Hanks,[14] C. Harper,[44] K. Hashimoto,[55,57] E. Haslum,[39] R. Hayano,[12] X. He,[20] T.K. Hemmick,[60] T. Hester,[8] J.C. Hill,[27] R.S. Hollis,[8] W. Holzmann,[14] K. Homma,[22] B. Hong,[31] T. Horaguchi,[63] Y. Hori,[12] D. Hornback,[51] S. Huang,[64] T. Ichihara,[55,56] R. Ichimiya,[55] H. Iinuma,[30] Y. Ikeda,[63] K. Imai,[28,33,55] M. Inaba,[63] A. Iordanova,[8] D. Isenhower,[1] M. Ishihara,[55] M. Issah,[64] D. Ivanischev,[54] Y. Iwanaga,[22] B.V. Jacak,[60] J. Jia,[7,59] X. Jiang,[37] D. John,[61] B.M. Johnson,[7] T. Jones,[1] K.S. Joo,[45] D. Jouan,[52] J. Kamin,[60] S. Kaneti,[60] B.H. Kang,[21] J.H. Kang,[67] J.S. Kang,[21] J. Kapustinsky,[37] K. Karatsu,[33,55] M. Kasai,[55,57] D. Kawall,[41,56] A.V. Kazantsev,[32] T. Kempel,[27] A. Khanzadeev,[54] K.M. Kijima,[22] B.I. Kim,[31] D.J. Kim,[29] E.-J. Kim,[10] Y.-J. Kim,[24] Y.K. Kim,[21] E. Kinney,[13] Á. Kiss,[17] E. Kistenev,[7] D. Kleinjan,[8] P. Kline,[60] L. Kochenda,[54] B. Komkov,[54] M. Konno,[63] J. Koster,[24] D. Kotov,[54] A. Král,[15] G.J. Kunde,[37] K. Kurita,[55,57] M. Kurosawa,[55] Y. Kwon,[67] G.S. Kyle,[49] R. Lacey,[59] Y.S. Lai,[14] J.G. Lajoie,[27] A. Lebedev,[27] D.M. Lee,[37] J. Lee,[18] K.B. Lee,[31] K.S. Lee,[31] S.H. Lee,[60] S.R. Lee,[10] M.J. Leitch,[37] M.A.L. Leite,[58] X. Li,[11] S.H. Lim,[67] L.A. Linden Levy,[13] H. Liu,[37] M.X. Liu,[37] B. Love,[64] D. Lynch,[7] C.F. Maguire,[64] Y.I. Makdisi,[6] A. Manion,[60] V.I. Manko,[32] E. Mannel,[14] Y. Mao,[53,55] H. Masui,[63] M. McCumber,[13,60] P.L. McGaughey,[37] D. McGlinchey,[13,19] C. McKinney,[24] N. Means,[60] M. Mendoza,[8] B. Meredith,[24] Y. Miake,[63] T. Mibe,[30] A.C. Mignerey,[40] K. Miki,[55,63] A. Milov,[65] J.T. Mitchell,[7] Y. Miyachi,[55,62] A.K. Mohanty,[4] H.J. Moon,[45] Y. Morino,[12] A. Morreale,[8] D.P. Morrison,[7,†] S. Motschwiller,[44] T.V. Moukhanova,[32] T. Murakami,[33] J. Murata,[55,57] S. Nagamiya,[30,55] J.L. Nagle,[13,‡] M. Naglis,[65] M.I. Nagy,[66] I. Nakagawa,[55,56] Y. Nakamiya,[22] K.R. Nakamura,[33,55] T. Nakamura,[55] K. Nakano,[55] J. Newby,[36] M. Nguyen,[60] M. Nihashi,[22] R. Nouicer,[7] A.S. Nyanin,[32] C. Oakley,[20] E. O'Brien,[7] C.A. Ogilvie,[27] M. Oka,[63] K. Okada,[56] A. Oskarsson,[39] M. Ouchida,[22,55] K. Ozawa,[12] R. Pak,[7] V. Pantuev,[25,60] V. Papavassiliou,[49] B.H. Park,[21] I.H. Park,[18] S.K. Park,[31] S.F. Pate,[49] L. Patel,[20] H. Pei,[27] J.-C. Peng,[24] H. Pereira,[16] D.Yu. Peressounko,[32] R. Petti,[7,60] C. Pinkenburg,[7] R.P. Pisani,[7] M. Proissl,[60] M.L. Purschke,[7] H. Qu,[20] J. Rak,[29] I. Ravinovich,[65] K.F. Read,[51,61] K. Reygers,[43] V. Riabov,[54] Y. Riabov,[54] E. Richardson,[40] D. Roach,[64] G. Roche,[38] S.D. Rolnick,[8] M. Rosati,[27] S.S.E. Rosendahl,[39] J.G. Rubin,[42] B. Sahlmueller,[43,60] N. Saito,[30] T. Sakaguchi,[7] V. Samsonov,[54] S. Sano,[12] M. Sarsour,[20] T. Sato,[63] M. Savastio,[60] S. Sawada,[30] K. Sedgwick,[8] R. Seidl,[56] R. Seto,[8] D. Sharma,[65] I. Shein,[23] T.-A. Shibata,[55,62] K. Shigaki,[22] H.H. Shim,[31] M. Shimomura,[63] K. Shoji,[33,55] P. Shukla,[4] A. Sickles,[7] C.L. Silva,[27] D. Silvermyr,[51] C. Silvestre,[16] K.S. Sim,[31] B.K. Singh,[3] C.P. Singh,[3] V. Singh,[3] M. Slunečka,[9] T. Sodre,[44] R.A. Soltz,[36] W.E. Sondheim,[37] S.P. Sorensen,[61] I.V. Sourikova,[7] P.W. Stankus,[51] E. Stenlund,[39] S.P. Stoll,[7] T. Sugitate,[22] A. Sukhanov,[7] J. Sun,[60] J. Sziklai,[66] E.M. Takagui,[58] A. Takahara,[12] A. Taketani,[55,56] R. Tanabe,[63] Y. Tanaka,[46] S. Taneja,[60] K. Tanida,[33,55,56] M.J. Tannenbaum,[7] S. Tarafdar,[3] A. Taranenko,[47,59] E. Tennant,[49] H. Themann,[60] D. Thomas,[1] M. Togawa,[56] L. Tomášek,[26] M. Tomášek,[26] H. Torii,[22] R.S. Towell,[1] I. Tserruya,[65] Y. Tsuchimoto,[22] K. Utsunomiya,[12] C. Vale,[7] H.W. van Hecke,[37] E. Vazquez-Zambrano,[14] A. Veicht,[14] J. Velkovska,[64] R. Vértesi,[66] M. Virius,[15] A. Vossen,[24] V. Vrba,[26] E. Vznuzdaev,[54] X.R. Wang,[49] D. Watanabe,[22] K. Watanabe,[63] Y. Watanabe,[55,56] Y.S. Watanabe,[12] F. Wei,[27] R. Wei,[59] J. Wessels,[43] S.N. White,[7] D. Winter,[14] C.L. Woody,[7] R.M. Wright,[1] M. Wysocki,[13] Y.L. Yamaguchi,[12,55] R. Yang,[24] A. Yanovich,[23] J. Ying,[20] S. Yokkaichi,[55,56] J.S. Yoo,[18]

Z. You,[37,53] G.R. Young,[51] I. Younus,[35,48] I.E. Yushmanov,[32] W.A. Zajc,[14] A. Zelenski,[6] and S. Zhou[11]
(PHENIX Collaboration)

[1]*Abilene Christian University, Abilene, Texas 79699, USA*
[2]*Department of Physics, Augustana College, Sioux Falls, South Dakota 57197, USA*
[3]*Department of Physics, Banaras Hindu University, Varanasi 221005, India*
[4]*Bhabha Atomic Research Centre, Bombay 400 085, India*
[5]*Baruch College, City University of New York, New York, New York, 10010 USA*
[6]*Collider-Accelerator Department, Brookhaven National Laboratory, Upton, New York 11973-5000, USA*
[7]*Physics Department, Brookhaven National Laboratory, Upton, New York 11973-5000, USA*
[8]*University of California - Riverside, Riverside, California 92521, USA*
[9]*Charles University, Ovocný trh 5, Praha 1, 116 36, Prague, Czech Republic*
[10]*Chonbuk National University, Jeonju, 561-756, Korea*
[11]*Science and Technology on Nuclear Data Laboratory, China Institute of Atomic Energy, Beijing 102413, People's Republic of China*
[12]*Center for Nuclear Study, Graduate School of Science, University of Tokyo, 7-3-1 Hongo, Bunkyo, Tokyo 113-0033, Japan*
[13]*University of Colorado, Boulder, Colorado 80309, USA*
[14]*Columbia University, New York, New York 10027 and Nevis Laboratories, Irvington, New York 10533, USA*
[15]*Czech Technical University, Zikova 4, 166 36 Prague 6, Czech Republic*
[16]*Dapnia, CEA Saclay, F-91191, Gif-sur-Yvette, France*
[17]*ELTE, Eötvös Loránd University, H-1117 Budapest, Pázmany Péter sétány 1/A, Hungary*
[18]*Ewha Womans University, Seoul 120-750, Korea*
[19]*Florida State University, Tallahassee, Florida 32306, USA*
[20]*Georgia State University, Atlanta, Georgia 30303, USA*
[21]*Hanyang University, Seoul 133-792, Korea*
[22]*Hiroshima University, Kagamiyama, Higashi-Hiroshima 739-8526, Japan*
[23]*IHEP Protvino, State Research Center of Russian Federation, Institute for High Energy Physics, Protvino, 142281, Russia*
[24]*University of Illinois at Urbana-Champaign, Urbana, Illinois 61801, USA*
[25]*Institute for Nuclear Research of the Russian Academy of Sciences, prospekt 60-letiya Oktyabrya 7a, Moscow 117312, Russia*
[26]*Institute of Physics, Academy of Sciences of the Czech Republic, Na Slovance 2, 182 21 Prague 8, Czech Republic*
[27]*Iowa State University, Ames, Iowa 50011, USA*
[28]*Advanced Science Research Center, Japan Atomic Energy Agency, 2-4 Shirakata Shirane, Tokai-mura, Naka-gun, Ibaraki-ken 319-1195, Japan*
[29]*Helsinki Institute of Physics and University of Jyväskylä, P.O.Box 35, FI-40014 Jyväskylä, Finland*
[30]*KEK, High Energy Accelerator Research Organization, Tsukuba, Ibaraki 305-0801, Japan*
[31]*Korea University, Seoul, 136-701, Korea*
[32]*Russian Research Center "Kurchatov Institute," Moscow, 123098 Russia*
[33]*Kyoto University, Kyoto 606-8502, Japan*
[34]*Laboratoire Leprince-Ringuet, Ecole Polytechnique, CNRS-IN2P3, Route de Saclay, F-91128, Palaiseau, France*
[35]*Physics Department, Lahore University of Management Sciences, Lahore 54792, Pakistan*
[36]*Lawrence Livermore National Laboratory, Livermore, California 94550, USA*
[37]*Los Alamos National Laboratory, Los Alamos, New Mexico 87545, USA*
[38]*LPC, Université Blaise Pascal, CNRS-IN2P3, Clermont-Fd, 63177 Aubiere Cedex, France*
[39]*Department of Physics, Lund University, Box 118, SE-221 00 Lund, Sweden*
[40]*University of Maryland, College Park, Maryland 20742, USA*
[41]*Department of Physics, University of Massachusetts, Amherst, Massachusetts 01003-9337, USA*
[42]*Department of Physics, University of Michigan, Ann Arbor, Michigan 48109-1040, USA*
[43]*Institut fur Kernphysik, University of Muenster, D-48149 Muenster, Germany*
[44]*Muhlenberg College, Allentown, Pennsylvania 18104-5586, USA*
[45]*Myongji University, Yongin, Kyonggido 449-728, Korea*
[46]*Nagasaki Institute of Applied Science, Nagasaki-shi, Nagasaki 851-0193, Japan*
[47]*National Research Nuclear University, MEPhI, Moscow Engineering Physics Institute, Moscow, 115409, Russia*
[48]*University of New Mexico, Albuquerque, New Mexico 87131, USA*
[49]*New Mexico State University, Las Cruces, New Mexico 88003, USA*
[50]*Department of Physics and Astronomy, Ohio University, Athens, Ohio 45701, USA*
[51]*Oak Ridge National Laboratory, Oak Ridge, Tennessee 37831, USA*
[52]*IPN-Orsay, Universite Paris Sud, CNRS-IN2P3, BP1, F-91406, Orsay, France*
[53]*Peking University, Beijing 100871, People's Republic of China*
[54]*PNPI, Petersburg Nuclear Physics Institute, Gatchina, Leningrad Region, 188300, Russia*
[55]*RIKEN Nishina Center for Accelerator-Based Science, Wako, Saitama 351-0198, Japan*
[56]*RIKEN BNL Research Center, Brookhaven National Laboratory, Upton, New York 11973-5000, USA*
[57]*Physics Department, Rikkyo University, 3-34-1 Nishi-Ikebukuro, Toshima, Tokyo 171-8501, Japan*
[58]*Universidade de São Paulo, Instituto de Física, Caixa Postal 66318, São Paulo CEP05315-970, Brazil*
[59]*Chemistry Department, Stony Brook University, SUNY, Stony Brook, New York 11794-3400, USA*

[60]Department of Physics and Astronomy, Stony Brook University, SUNY, Stony Brook, New York 11794-3800, USA
[61]University of Tennessee, Knoxville, Tennessee 37996, USA
[62]Department of Physics, Tokyo Institute of Technology, Oh-okayama, Meguro, Tokyo 152-8551, Japan
[63]Institute of Physics, University of Tsukuba, Tsukuba, Ibaraki 305, Japan
[64]Vanderbilt University, Nashville, Tennessee 37235, USA
[65]Weizmann Institute, Rehovot 76100, Israel
[66]Institute for Particle and Nuclear Physics, Wigner Research Centre for Physics, Hungarian Academy of Sciences (Wigner RCP, RMKI) H-1525 Budapest 114, POBox 49, Budapest, Hungary
[67]Yonsei University, IPAP, Seoul 120-749, Korea

We present midrapidity charged-pion invariant cross sections, the ratio of the π^- to π^+ cross sections and the charge-separated double-spin asymmetries in polarized p+p collisions at $\sqrt{s}$ = 200 GeV. While the cross section measurements are consistent within the errors of next-to-leading-order (NLO) perturbative quantum chromodynamics predictions (pQCD), the same calculations over estimate the ratio of the charged-pion cross sections. This discrepancy arises from the cancellation of the substantial systematic errors associated with the NLO-pQCD predictions in the ratio and highlights the constraints these data will place on flavor dependent pion fragmentation functions. The charge-separated pion asymmetries presented here sample an x range of ∼0.03–0.16 and provide unique information on the sign of the gluon-helicity distribution.

PACS numbers: Valid PACS appear here

I. INTRODUCTION

Quantum chromodynamics (QCD) is well established as the theory of the strong interaction, yet it is expressed in terms of quarks and gluons, which are confined in color-neutral hadrons and are not observed in isolation. While high-energy scattering of quarks and gluons is calculable perturbatively from theory alone, perturbative calculations cannot be used without experimental input to determine the quark and gluon structure of QCD bound states or the process of hadronization of a scattered quark or gluon. Performing high-energy experimental measurements involving hadrons permits the study of nonperturbative aspects of QCD supported by the robust and directly calculable framework of perturbative QCD (pQCD). In particular, hadron structure can be described in terms of parton distribution functions (PDFs), and parton hadronization in terms of fragmentation functions (FFs). These nonperturbative, or long-distance, descriptions factorize from the perturbative, or short-distance, partonic hard scattering process, and they are universal across different observable reactions.

A great deal about nucleon structure has been learned from experimental measurements of inclusive deep-inelastic lepton-nucleon scattering (DIS), with complementary knowledge gained from other scattering processes. Proton-proton scattering to produce jets, hadrons, or direct photons provides access to gluons at leading order in pQCD. The dependence of inclusive DIS on the hard momentum scale of the scattering, Q^2, offers an additional handle on gluon distributions for observables measured over a wide range of hard scales.

Different experimental measurements allow access to different aspects of proton structure. Measurements involving unpolarized protons and a single observed hard momentum scale, enabling the framework of pQCD to be employed, constrain the unpolarized collinear PDFs; measurements involving longitudinally polarized protons and a single hard scale constrain helicity-dependent collinear PDFs. For recent reviews on nucleon structure, see [1–5].

The Relativistic Heavy Ion Collider (RHIC) is an extremely versatile hadronic collider, having achieved collisions of ion species from protons to uranium over an energy range from a few GeV to several hundred GeV. With the ability to control the polarization direction of proton beams from 25 to 255 GeV, corresponding to center-of-mass energies of 50 to 510 GeV, RHIC is excellently suited to study numerous aspects of nucleon structure. One of the main goals of the nucleon structure program at RHIC has been to better constrain the helicity PDFs of the proton, given that experimental measurements indicate that only 25–35% of the proton's longitudinal spin is carried by the quark spins [6–10], significantly less than the prediction based on the simple parton model [11].

According to the Jaffe-Manohar sum rule for the spin of the proton [12], the proton's longitudinal spin can be decomposed as $\frac{1}{2} = \frac{1}{2}\Delta\Sigma + \Delta G + L_q + L_g$, where $\frac{1}{2}\Delta\Sigma$ is the net quark and antiquark spin, ΔG is the net gluon spin, and $L_q + L_g$ is the orbital angular momentum of partons. Within the Jaffe-Manohar decomposition, it is known how to compare $\Delta\Sigma$ and ΔG to experimental measurements as they are gauge invariant. Particularly, ΔG has a physical interpretation as gluon spin in the light cone gauge. For a recent review of helicity sum rules and the interpretations of their components, see [13, 14].

RHIC measurements of the double-longitudinal spin asymmetry in the production of hadrons [15–17] and jets [18–20], as well as single-longitudinal spin asymmetry measurements in the production of W bosons [21–23], have already

*Deceased
†PHENIX Co-Spokesperson: morrison@bnl.gov
‡PHENIX Co-Spokesperson: jamie.nagle@colorado.edu

been used in helicity PDF fits [24–28].

Using hadrons in the final state to study nucleon structure, i.e. in the processes of $p+p$ to hadrons or SIDIS, requires knowledge of FFs. Fragmentation functions are in a sense complementary to PDFs. While PDFs describe the behavior of colored quarks and gluons bound in a colorless hadron, FFs describe a colored quark or gluon transitioning into one or more colorless hadrons. As in the case of PDFs, different experimental measurements can provide a variety of information on FFs. Much has been learned from the process of electron-positron annihilation to hadrons, while $p+p$ collisions are especially useful in constraining gluon FFs, and SIDIS data can provide information on quark flavor. Hadron production in $p+p$ collisions offers additional flavor sensitivity, and the Q^2 evolution of hadrons produced in e^+e^- provides an additional handle on gluons. Cross section measurements of inclusive hadron production at RHIC [29–34] have already been used to help constrain FFs for charged and neutral pions and kaons, protons, and lambdas [35–39]. Measurements of back-to-back direct photon and charged hadron production to study hadronization in $p+p$ collisions at RHIC have also been performed [40]. For a review of FFs, see [41].

This paper presents charged-pion cross section measurements in polarization-averaged $p+p$ collisions and double-helicity asymmetry measurements in charged pion production in longitudinally polarized proton collisions at $\sqrt{s} =$ 200 GeV. The cross section measurements provide information on charge-separated collinear FFs for pions; the spin asymmetry measurements are sensitive to the collinear helicity distributions in the proton. Improved knowledge of FFs can lead to improved knowledge of PDFs, and vice versa, in a continuous, iterative process of increasingly refined constraints on nonperturbative aspects of QCD. In Sec. II we describe the PHENIX experiment; Sec. III discusses the analysis; Sec. IV presents the results, which are further discussed in Sec. V; and Sec. VI summarizes our findings.

II. THE PHENIX EXPERIMENT

A large set of data was taken in 2009 from polarized $p+p$ collisions at $\sqrt{s} = 200$ GeV, and an integrated luminosity of 11.8 pb^{-1} was analyzed for charged pion production at midrapidity. The PHENIX detector is configured with two central arm spectrometers each covering 90° in azimuth, $|\eta| < 0.35$ in pseudorapidity, two forward muon spectrometers (not discussed further) and two sets of detectors to determine collision parameters.

The central arms comprise several tracking layers composed of a drift chamber (DC) and pad chambers (PC), a ring-imaging Čerenkov (RICH) detector for particle identification, and an electromagnetic calorimeter (EMCal). In 2009, an additional Čerenkov detector, the hadron-blind detector (HBD), was added to reduce the combinatorial background in low-mass dilepton measurements in heavy ion collisions; this detector can also be used for charged pion identification. Results on single electrons from heavy flavor decays measured using the HBD have already been published [42]. A layout of the central arms is shown in Fig. 1.

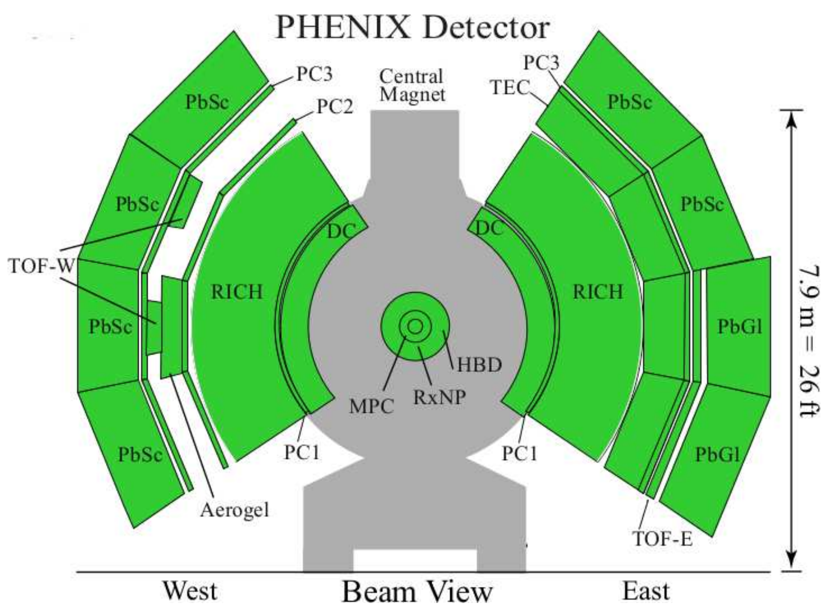

FIG. 1: (color online) Cross section view along the beam line of the PHENIX detector, showing the detectors composing the central arms described in the text, as well as the HBD added in 2009.

A. Collision Detectors

Two beam-beam counters (BBCs) [43] placed at 144 cm on either side of the interaction point (IP) of PHENIX along the beam axis were used for event start timing, triggering, luminosity monitoring and determination of the location of the collision vertex along the beam axis. The BBCs are built with 64 photomultiplier tubes, each coupled to a quartz Čerenkov radiator. An offline cut of 30 cm in the distribution of the reconstructed collision point was used for event selection.

Additionally, two zero-degree calorimeters (ZDCs) are located 18 m from the IP along the beam axis, after the RHIC beam bending magnets. Each ZDC comprises three sections of hadron calorimeter composed of optical fibers for Čerenkov sampling between layers of tungsten absorber. Between the first and second sections is placed a shower-maximum detector (SMD), which comprises vertical and horizontal scintillator strips, and is designed to determine the shower maximum of hadronic (primarily neutron) showers. The ZDCs are used as a comparison luminosity monitor and, with the SMD, to ensure transverse components of the beam polarization are small. Any remaining transverse components of the beam polarization can be determined by the transverse single-spin asymmetry observed for forward neutron production at RHIC [44].

B. Magnetic Field and Tracking Detectors

The central magnet [45] in PHENIX supplies an axial field for momentum measurements of charged particles. It comprises two coils, the inner and outer, which can be run independently. To have a field free region in the HBD volume in 2009, the coils were run in an opposing '$+-$' configuration. In this configuration, the field strength is near zero for $0 < R < 50$ cm, corresponding to the HBD region, and then increases to a peak of 0.35 T around 1 m, with a total magnetic field integral of 0.43 Tm. It is designed such that the field strength is near zero at 2 m, where the first tracking layers are located, and is required to be less than 100 Gauss in the region of the RICH photomultiplier tubes.

The primary tracking device to determine momentum is the DC [46], located radially between 2 and 2.5 m from the z-axis in a region of low magnetic field strength. The transverse component of the track momentum with respect to the beam particle direction is determined based on the angle between the reconstructed track, after bending in the magnetic field, and the straight line from the z-axis to the track midpoint in the DC. The first layer of the PC detector [46] (PC1) sits behind the DC radially, and is used along with the reconstructed collision vertex to determine the component of the momentum parallel to the z-axis. A third layer of the PC (PC3) is located radially directly in front of the EMCal, and is used to ensure track quality.

C. Electromagnetic Calorimeter

The EMCal [47] was used for triggering. Six of the eight EMCal sectors are constructed from lead-scintillator (PbSc) towers in a sampling configuration while the remaining two sectors are made of lead-glass (PbGl) towers. The PbSc (PbGl) EMCal corresponds to 0.85 (1.05) nuclear interaction lengths.

A high energy trigger, primarily designed for photons, is implemented in the EMCal, and was used to select high momentum charged pion candidates. Events were triggered by requiring an EMCal cluster with an energy threshold of 1.4 GeV in addition to a BBC coincidence trigger.

D. Charged Pion Identification

In 2009, PHENIX had two Čerenkov based charged particle identification detectors: the RICH and the HBD. While both were primarily designed to identify electrons, they can also be used to identify pions above $p_T \sim 4.7$ GeV/c.

The RICH [48], which uses CO_2 as a radiator, allows for the identification of charged pions above $p_T \sim 4.7$ GeV/c. The Čerenkov light is collected by a photomultiplier array on a plane outside of the tracking acceptance after reflection by a pair of focusing spherical mirrors.

The HBD [49] is a gas electron multiplier (GEM) based Čerenkov detector. Located at $\sim$5 cm from the beam pipe with the windowless CF_4 radiator extending to $\sim$60 cm in the radial direction, it covered a pseudorapidity range of $|\eta|<0.45$. The p_T thresholds of Čerenkov radiation for electrons, pions, and kaons in CF_4 are $\sim 1, 4$, and 14 GeV/c, respectively. The Čerenkov photons generate photoelectrons on a CsI photocathode layer on the first GEM foil which are subsequently amplified as they traverse the GEM holes and collected in readout pads. Because electrons produced in the avalanche can be distributed over more than one readout pad, adjacent pads with charge above the pedestal are grouped together to form a cluster. The total cluster charge is used as a variable for particle identification. In addition to Čerenkov photons, scintillation photons can also be generated by charged particles moving inside the radiator. The mean number of photons created by scintillation per charged particle ($\sim$1) is much smaller than that created through Čerenkov radiation. At $p_T > 5$ GeV/c, electrons produce a mean of 20 photoelectrons while the yield for pions has a p_T dependence due to the high threshold momentum.

III. DATA ANALYSIS

Charged pion candidates are selected based on track quality and particle identification cuts in the Čerenkov detectors. Each candidate is required to have a high quality, unique track defined in the DC and an associated PC1 hit. Further, the track is required to match with hits in the PC3 and EMCal. Candidate tracks are required to be associated with an EMCal trigger. For the RICH, we define the variable, n_1, as the total number of photomultipliers that fired within a radius of 11 cm around the projected track position. For charged pion candidates, we require $n_1 > 0$. Note that this cut is not intended for rejection of electrons, but rather heavier hadrons that do not radiate in the RICH.

A further cut is applied based on the HBD cluster charge. Figure 2 shows the HBD cluster charge distribution of $\pi^{\pm}$ candidates after applying all cuts other than the HBD cluster charge cut. The cluster charge distributions for four p_T bins are shown in Fig. 2(a). The peak on the right for each p_T bin is from $\pi^{\pm}$. The mean number of photoelectrons generated before avalanche is extracted for each peak by fitting the charge distribution with a statistical model distribution known as the folded-Polya probability distribution. The analytic form of the folded Polya distribution is derived from the Polya distribution by convolution with an avalanche process model. Fitting results consistently describe the rising mean number of Čerenkov photons with p_T. The secondary peak found on the left comes from scintillations in the HBD. A sum of two folded-Polya functions with independent weights was used as a fit function for the whole charge distribution. An example of fitted cluster charge distribution is shown in Fig. 2(b).

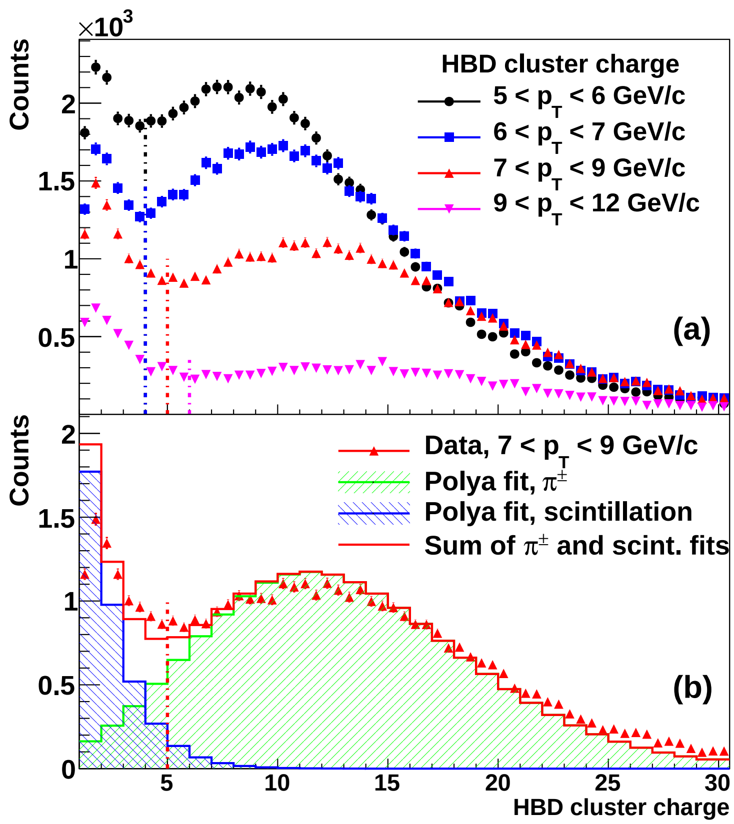

FIG. 2: (color online) The HBD cluster charge distribution, in units of photoelectrons. Cuts applied on the cluster charge for the four p_T bins are shown as dashed lines. Note that the cluster charge cut for tracks reconstructed with 5–6 and 6–7 GeV/c was the same.

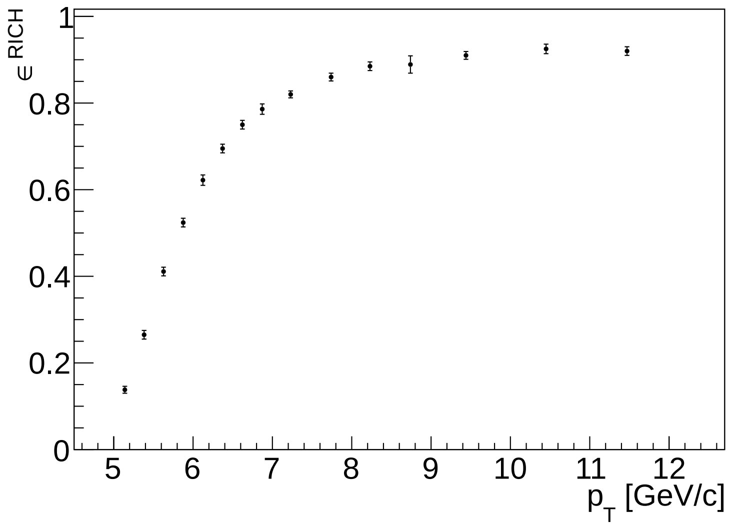

FIG. 3: The RICH efficiency as a function of pion p_T above the pion Čerenkov threshold in the RICH.

Tracks accidentally associated with scintillation charge on the HBD mainly comprise electrons from photon conversions and from decays of long lived hadrons outside the HBD. As the first tracking detectors sit outside of the magnetic field region, the momentum of such electrons created far from the collision point will be incorrectly reconstructed, and then may be incorrectly associated with a track-matching cluster charge in the HBD. Applying p_T-dependent cuts on the cluster charge (vertical lines in Fig. 2) resulted in effective removal of these incorrectly reconstructed electrons. Residual background after applying these cuts is estimated by taking the count ratio of the scintillation to the pion contribution above the charge cut. Compared with the analysis without the HBD, inclusion of the HBD in particle identification resulted in improvement in this background source from $\sim$ 30% to <2% averaged over the p_T range.

The only remaining background that could pass the requirement of a Čerenkov cluster in the HBD is electrons created prior to the HBD back plane, such as from decays of neutral pions (dominant), K_{e3} electrons ($K^{\pm}/K_L \rightarrow \pi^0 e^{\pm} \nu$), heavy flavor and vector mesons. As such electrons are generated prior to traversing the magnetic field region, their reconstructed momentum is generally correct. However, these contributions are suppressed due to small cross sections and small branching ratios in the case of heavy flavor and vector mesons, and small conversion or decay probabilities inside the HBD for electrons from π^0 and K_{e3}. In the case of decay electrons, decay kinematics further reduces their rate because the p_T distribution of decay electrons is softer than that of the parent particles. The rate of electrons from the largest contributors (conversion of π^0-decay photons and π^0 Dalitz decay) evaluated by these considerations of cross sections and branching ratios amount to $\lesssim$ 2.7% of the rate of signal events, while other sources combined are less than 1%.

For a cross section measurement, the track reconstruction efficiencies must be determined. For this measurement, we have separated the geometric acceptance, which is determined from MC simulations, and detector efficiencies, which are determined from data. The systematic uncertainty of the geometric acceptance was determined to be 2% by varying the boundary of the active detection area in the simulation.

For determination of detector efficiencies, we calculate the survival probability, when requiring a hit in the active area of a detector, of a sample of clean $\pi^{\pm}$ tracks that leave a signal in all other detectors. This sample was acquired by using tighter cuts to enhance the signal fraction. First, dead areas were identified by comparing hit and projected track distributions and masked. This was done to obtain pure detector efficiencies, not convoluted with dead area effect. Data were then divided into groups to account for the variation of efficiency with time. Within each group, the weighted average of the fill-by-fill efficiency was used as an effective efficiency, with the RMS assigned as the systematic uncertainty (2.8% for the DC, 4.5% for the PC and 1.6% for the HBD).

For the RICH, using the method described in the previous paragraph is particularly advantageous as it allows measuring the sharply rising efficiency near the Čerenkov threshold in a model-independent way. Model based MC simulations do not well describe this efficiency turn-on. Figure 3 shows the measured RICH efficiency as a function of p_T showing a clear rise above the RICH Čerenkov threshold for pions. The systematic uncertainties on the RICH efficiency were determined by comparing with a Fermi function used to describe the turn on, and varied from 12% at 5 GeV/c to $\sim$1% at high p_T.

The momentum smearing effect caused by finite resolution of measured p_T was corrected by unfolding the measured cross section using the Singular Value Decomposition method [50]. The unfolded p_T distribution corresponds to the true p_T distribution given that the p_T was affected by the resolution function of PHENIX tracking system, found to be $\sqrt{(1.74)^2 + (1.48 \times p_T[\mathrm{GeV}/c])^2}\%$. The constant term is due to multiple scattering of charged tracks in the detector material and the linear term is caused by the intrinsic hit position resolution of the DC. The hardening factors of the p_T spectra, determined p_T bin by p_T bin by taking the ratio between the fitted curves of the unfolded p_T distribution and the measured cross section, were negligible below 8 GeV/c but become significant ($\sim 16\%$) at the highest p_T bin due to the sufficiently large p_T resolution. The systematic uncertainty from momentum smearing was estimated to be 1% by comparing the fitted curves of measured cross section and the re-smeared spectra of unfolded results. The corrections on the cross section measurements attributed to the momentum smearing effect are large due to the rapidly falling shape of the cross section. However, the impact of momentum smearing on the A_{LL} asymmetry measurements can be ignored as the asymmetries vary much more slowly as a function of p_T.

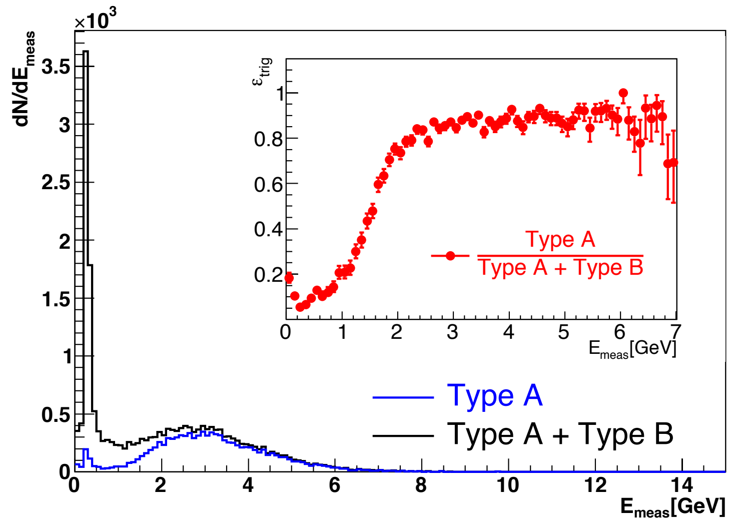

FIG. 4: (color online) The energy spectra of (black) all charged pions (type A+type B) and (blue) those that fire the EMCal trigger (type A). The inset shows the resulting EMCal trigger efficiency for charged pions as a function of deposited energy.

The trigger efficiency is an important absolute normalization factor in the measurement of invariant differential cross sections. As PHENIX does not have a dedicated charged hadron trigger, a new method was developed to determine the EMCal trigger efficiency for charged pions to cause the trigger. This method exploits the event structure to select a high statistics subset of the data from which the EMCal trigger bias is removed. This subset is composed of events containing a high p_T charged pion in addition to one or more spatially separated particles which fired the EMCal trigger. To avoid possible bias from a trigger associated with a nearby particle, a minimum energy cut of 0.2 GeV was applied to both the charged pion and the associated particle that fired the trigger. These events are divided into two types: type A where the pion does fire the trigger and type B otherwise. Figure 4 shows the spectra for all pions in black and type A–those that fire the trigger–in blue. We define the trigger efficiency as the ratio of type A event counts to the sum of type A and type B event counts (i.e., all events) above the minimum energy cutoff. The inset in Fig. 4 shows this ratio as a function of the deposited energy in the EMCal for charged pions of $5 < p_T < 13$ GeV/c. The average trigger efficiency for all energies above the cutoff was also calculated as a function of p_T, and shows no p_T dependence. A constant fit over the whole p_T range yields value of 0.497±0.7% for the trigger efficiency with a χ^2/d.o.f.=0.88.

The full list of systematic uncertainties associated with the correction factors discussed so far is summarized in Table I. The systematic uncertainties reported for the ratio of the cross sections of π^+ to π^- are calculated as the quadratic sum of those uncertainties that do not cancel out between the two measurements. A systematic uncertainty is considered to cancel between the two measurements if a change in the underlying cause modifies the cross sections of π^- and π^+ by the same multiplicative factor. This is the case for instance with all the uncertainties related to the efficiency of individual detectors. A misdetermination of these efficiencies would affect the π^+ and π^- cross sections identically, hence its effect would not be visible in the ratio. However, the geometric acceptance uncertainties do not cancel for the two charges. This is because the way dead areas are seen by tracks of opposite signs are different, and hence, a change in detector dead area configuration will not affect the geometrical acceptances in the same way for π^+ and π^-. The same is true for the p_T smearing correction uncertainty. These are the only two uncertainties considered in the ratio measurement.

TABLE I: Summary of systematic uncertainties for each p_T bin (in %) The $\epsilon^{\mathrm{reco}}_{\mathrm{DET}}$ stands for the reconstruction efficiency of each detector used for this analysis, while the remaining three uncertainties are related to geometrical acceptance correction $\epsilon^{\mathrm{geo}}_{\mathrm{acc}}$, trigger efficiency correction $\epsilon^{\mathrm{trig.}}_{\mathrm{eff.}}$, and p_T smearing correction $\epsilon^{p_T}_{\mathrm{smear}}$

p_T bin (GeV/c)	$\epsilon^{\mathrm{reco}}_{\mathrm{DC}}$	$\epsilon^{\mathrm{reco}}_{\mathrm{HBD}}$	$\epsilon^{\mathrm{reco}}_{\mathrm{PC3}}$	$\epsilon^{\mathrm{reco}}_{\mathrm{RICH}}$	$\epsilon^{\mathrm{geo.}}_{\mathrm{acc.}}$	$\epsilon^{\mathrm{trig.}}_{\mathrm{eff.}}$	$\epsilon^{p_T}_{\mathrm{smear}}$
5–6	2.8	1.6	4.5	12.1	2.0	1.4	1.0
6–7	2.8	1.6	4.5	2.6	2.0	1.2	1.0
7–8	2.8	1.6	4.5	0.9	2.0	1.6	1.0
8–9	2.8	1.6	4.5	0.6	2.0	2.2	1.0
9–11	2.8	1.6	4.5	0.5	2.0	2.3	1.0
11–13	2.8	1.6	4.5	0.5	2.0	5.1	1.0

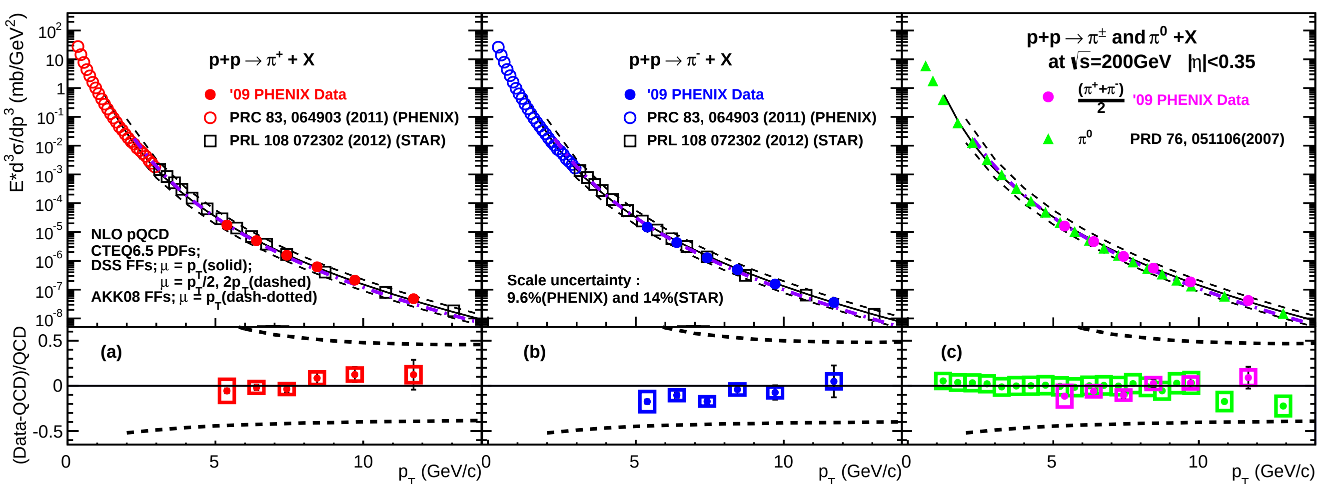

FIG. 5: (color online) Invariant cross sections for (a) π^+ and (b) π^- with pQCD predictions using the DSS [35] and AKK08 [37] FFs. Top panel: PHENIX [51] and STAR [52] results are also compared. Bottom: systematic (boxes) and statistical (bars) uncertainties are shown with relative difference between data and prediction. (c) Comparison of averaged charged pion cross section and π^0 cross section by PHENIX [53]. Bottom panel: data-theory comparisons.

IV. RESULTS

A. Cross Sections

The cross section measurements for π^+ and π^- hadrons are shown in Fig. 5(a) and (b), respectively, along with previously published PHENIX results [51] for low-p_T charged pions measured with the PHENIX Time of Flight detector [48], which can identify pions for $p_T < 3$ GeV/c. There is an overall scale uncertainty from the determination of the absolute luminosity sampled of 9.6%, correlated between all PHENIX results. This absolute normalization uncertainty derives from the uncertainty on the inelastic p+p cross section sampled by the BBC trigger, which is found to be 23.0±2.2 mb based on van der Meer scan results [29] corrected for year-to-year variations in the BBC performance. Results from the STAR experiment [52] are also plotted and are consistent with the new PHENIX data.

In Fig. 5(c), the charge-averaged pion cross section is shown along with the previously published PHENIX neutral pion cross section [53]. The charged and neutral pion measurement are found to be in good agreement with each other, as can be seen in the lower panel where both are compared to pQCD calculations [54]. The comparison of the measurements to the theoretical calculations is discussed further in Sec. V below.

TABLE II: Invariant cross section for π^+ and π^- hadrons, as well as the statistical and systematic uncertainties. In addition, there is an absolute scale uncertainty of 9.6%.

			π^+			π^-	
p_T bin (GeV/c)	$\langle p_T \rangle$ (GeV/c)	$E * \frac{d^3\sigma}{dp^3}$ (mb/GeV^2)	STAT	SYST	$E * \frac{d^3\sigma}{dp^3}$ (mb/GeV^2)	STAT	SYST
5–6	5.39	1.75×10^{-5}	0.05×10^{-5}	0.24×10^{-5}	1.49×10^{-5}	0.04×10^{-5}	0.20×10^{-5}
6–7	6.39	5.01×10^{-6}	0.15×10^{-6}	0.33×10^{-6}	4.30×10^{-6}	0.13×10^{-6}	0.29×10^{-6}
7–8	7.41	1.56×10^{-6}	0.07×10^{-6}	0.10×10^{-6}	1.283×10^{-6}	0.060×10^{-6}	0.080×10^{-6}
8–9	8.44	6.19×10^{-7}	0.39×10^{-7}	0.40×10^{-7}	4.94×10^{-7}	0.35×10^{-7}	0.32×10^{-7}
9–11	9.71	2.14×10^{-7}	0.16×10^{-7}	0.14×10^{-7}	1.57×10^{-7}	0.13×10^{-7}	0.10×10^{-7}
11–13	11.70	4.83×10^{-8}	0.71×10^{-8}	0.38×10^{-8}	3.57×10^{-8}	0.60×10^{-8}	0.28×10^{-8}

B. Cross Section Ratio

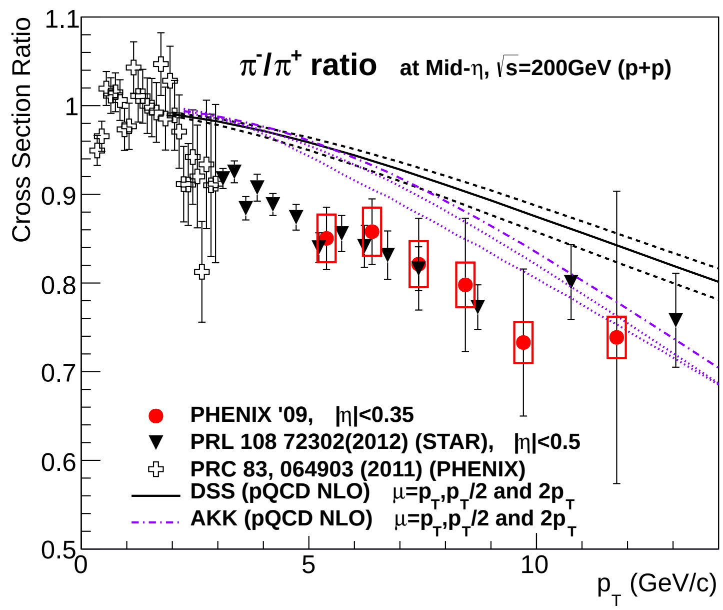

FIG. 6: (color online) The ratio of the pion production cross sections for the two charges. Systematic uncertainties are shown in red boxes. Also shown are the PHENIX low p_T results and the STAR high p_T results.

The π^--to-π^+ cross section ratio from this analysis is shown in Fig. 6 together with the measurements from PHENIX [51] at lower p_T and from STAR [52] in a similar p_T range. The results from the three measurements are compatible. The experimental data is compared to pQCD calculations based on DSS [35, 39] and AKK [37] FFs. The calculated ratio values for theory scale choices of $\mu = p_T$, $\mu = 0.5p_T$, and $\mu = 2p_T$ are additionally shown.

C. Helicity Asymmetries

Hard processes in polarized $p+p$ collisions allow us to directly probe gluons and thereby constrain the gluon helicity distribution $\Delta g(x, Q^2)$ which is related to the gluon spin via $\Delta G \equiv \int_0^1 dx\ \Delta g(x, Q^2)$. Experimentally, the observable used for this analysis is the double longitudinal spin asymmetry

$$A_{LL} \equiv \frac{\sigma^{++} - \sigma^{+-}}{\sigma^{++} + \sigma^{+-}}, \tag{1}$$

where $\sigma^{++(+-)}$ is the cross section with same (opposite) sign helicity states of the incoming protons. In pQCD, the numerator in Eq. 1 is proportional to $\Sigma_{ij}\Delta f_i \otimes \Delta f_j \otimes \Delta\hat{\sigma}_{ij} \otimes D_k^h$, where $\Delta f_{i(j)}$ are the helicity-dependent PDFs of parton type i (j) and depend on the partonic momentum fraction x and on the factorization scale μ_F, $\Delta\hat{\sigma} = \hat{\sigma}^{++} - \hat{\sigma}^{+-}$ is the polarized partonic cross section that depends on the renormalization scale μ_R and D_k^h is the FF for the hadronization of outgoing parton k, which is a function of the fragmentation scale $\mu_{F'}$. For particle production involving q-g or g-g partonic scattering processes, information on $\Delta g(x, Q^2)$ is encoded in Eq. 1.

The A_{LL} of various singly inclusive (single-particle/jet) and doubly inclusive (two-particle/jet) production are measured at RHIC. The recent addition of single-inclusive π^0 [15–17, 53] and jet A_{LL} [19, 55] measurements to a global analysis by de Florian, et al. (DSSV) [24, 25, 28] is starting to impose significant constraints on ΔG. However, improving systematic uncertainties at low p_T arising from experimental as well as theoretical sources remains a challenge. In addition, the complex nature of extracting PDFs and FFs by fitting data sets from various experiments demands independent measurements through the production of different final-state particles covering a wide kinematic range.

Single inclusive midrapidity charged pion production for $5 < p_T < 12$ GeV/c from 200 GeV p+p collisions is dominated by the q-g hard process [34] and the polarized partonic cross sections for all the relevant hard processes are positive. The signs of Δu and Δd are known to be positive and negative, respectively (see e.g. [24]). Also, u-quarks preferentially fragment into π^+ and d-quarks into π^-. Consequently, the double longitudinal spin asymmetries for the three π meson species should be ordered as $A_{LL}^{\pi^+} > A_{LL}^{\pi^0} > A_{LL}^{\pi^-}$ for a positive Δg and vice versa for a negative Δg in leading order pQCD.

A more quantitative interpretation requires the inclusion of such data into a global fit using the next-to-leading order (NLO) pQCD framework. The midrapidity production of charged pions with $5 < p_T < 12$ GeV/c at $\sqrt{s} = 200$ GeV covers the kinematic range of $0.03 \lesssim x \lesssim 0.16$. The relevant ingredients for a global analysis are available: unpolarized quark and gluon PDFs, polarized quark PDFs, charge-separated unpolarized FFs [35] and hard scattering cross sections at NLO. The invariant differential cross sections for π^+ and π^- as a function of p_T can be used to check the validity of the NLO pQCD calculation as well as the PDFs and FFs adopted for the global analysis on ΔG.

The double-spin asymmetry A_{LL} for inclusive charged pion production is measured as

$$A_{LL} = \frac{1}{\langle P_B \cdot P_Y \rangle} \frac{N^{++} - R \cdot N^{+-}}{N^{++} + R \cdot N^{+-}}, R = \frac{L^{++}}{L^{+-}} \tag{2}$$

where N is the number of charged pions and L is the luminosity for a given helicity combination. The notation $++$ ($+-$) follows the same convention as in Eq. 1. The polarizations of the two counter-circulating RHIC beams are denoted as P_B and P_Y and for 2009 were 0.56 and 0.55, respectively. The luminosity-weighted beam polarization product $\langle P_B P_Y \rangle$, important for A_{LL}, was 0.31 with a global relative scale uncertainty of 6.5% on the product. An additional uncertainty based on the precision with which we can determine the degree of longitudinal polarization in the collision [17] must be included, leading to a total relative scale uncertainty of $^{+7.0\%}_{-7.7\%}$.

The relative luminosity, R, between the sampled luminosities for the different helicities is determined from the yield of BBC triggered events on a fill-by-fill basis. The systematic uncertainty on relative luminosity is determined by comparing to the yield of ZDC triggers [17], and was found in 2009 to be 1.4×10^{-3}.

Beyond the systematic uncertainties from polarization and relative luminosity, the dominant systematic uncertainty on the asymmetries are from tracks misidentified as charged pions. The size of the possible asymmetry from this background was determined to be $\sim 10^{-4}$. The determination was performed by calculating the spin asymmetries of the subsample of charged tracks found in the vicinity of an HBD cluster whose charge is between 1 and 20. In order to randomize the association, the tracks in the sample were required to point to the reflected track projection with respect to the vertical plane passing through the beam line. The charge distribution of the HBD clusters randomly associated with the charged tracks in the sample exhibits the characteristic exponential decay of scintillation photons [49], ensuring that they are a good sample of tracks misidentified as pions.

Charge-separated pion A_{LL} measurements are shown in Fig. 7. As statistical errors dominate the uncertainties, point-to-point systematic errors are not plotted.

V. DISCUSSION

A. Cross Sections and Charge Ratio

In Fig. 5, the charged pion cross sections are compared to pQCD calculations [54] which were performed at NLO using CTEQ6.5 unpolarized PDFs [56] and DSS [35, 39] and AKK [37] FFs. In the bottom panel of each figure, the relative difference between data and theory is also shown for the DSS FFs. The absolute normalization uncertainty

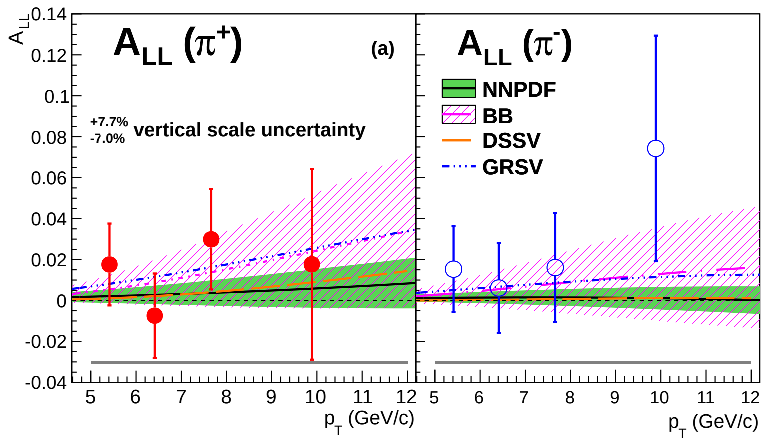

FIG. 7: (color online) The double-helicity asymmetries for (a) π^+ and (b) π^- produced in p+p collisions at $\sqrt{s}$ = 200 GeV for $|\eta| < 0.35$. The p_T-correlated systematic uncertainty from the relative luminosity is shown in gray. The $^{+7.0\%}_{-7.7\%}$ scaling uncertainty is from beam polarization.

TABLE III: Double-helicity asymmetries and statistical uncertainties for π^+ and π^- hadrons. The primary systematic uncertainties, which are fully correlated between points, are 1.4×10^{-3} from relative luminosity and a $^{+7.0\%}_{-7.7\%}$ scaling uncertainty from beam polarization.

		π^+		π^-	
p_T bin (GeV/c)	$\langle p_T \rangle$ (GeV/c)	A_{LL}	$STAT$	A_{LL}	$STAT$
5–6	5.41	0.018	0.020	0.015	0.021
6–7	6.41	-0.007	0.021	0.006	0.022
7–9	7.66	0.030	0.025	0.016	0.027
9–12	9.89	0.018	0.047	0.074	0.055

of 9.6% is not included in the systematic errors shown in boxes. A standard technique for determining theoretical uncertainties is to vary the renormalization, factorization, and fragmentation theory scales by a set factor, in this case 2. Here the three scales, denoted μ, are set to be equal, and are varied from $\mu = 0.5p_T$ to $\mu = 2p_T$. The pion measurements fall within $\sim \pm 20\%$ of the pQCD calculation at a scale of $\mu = p_T$, well within the much larger range defined by varying the scales. Note that no other uncertainties on the pQCD calculations such as those due to PDF uncertainties or FF uncertainties are included.

The measured ratio of π^--to-π^+ production is shown in Fig. 6. At low p_T where $\pi^\pm$ production is dominated by g-g scattering, the measured charge ratio of pion production is close to 1. In contrast, q-g scattering dominates $\pi^\pm$ production at higher p_T and the ratio starts to deviate from 1 due to the valence quark content of the proton. Any hadrons that fragment preferentially from u-quarks are enhanced with respect to hadrons that fragment preferentially from d-quarks, leading to an increase of positive with respect to negative pions. As presented in Fig. 6, the pQCD calculations of the π^--to-π^+ ratio lie above the measured ratio for p_T>$\sim$2–3 GeV/c by as much as $\sim$20% for both the DSS [35] and AKK [37] FFs. We note that the calculated midrapidity $\bar{p}$-to-p ratio using DSS FFs [36] exceeds the ratio measured by PHENIX by 20%–40% [51]. The theoretical curves shown are simply obtained by dividing the two cross section calculations for each of the different scales. The range of calculated ratios indicates disagreement with the measured ratio presented in this paper as well as that from STAR [52]; the discrepancy implies that other sources of uncertainty in the ratio calculation need to be investigated. Uncertainties for the DSS FFs are estimated in [39], but a calculation taking into account these uncertainties and which components cancel or do not cancel in the ratio is not currently available. Given extensive work in recent years to develop Lagrange multiplier and Hessian techniques to assess uncertainties on PDFs and FFs following early work by the CTEQ collaboration [57][58], the community should soon reach a point where it is standard to propagate PDF and FF uncertainties fully for calculations of observables. We note that much of the data used in the pion FFs comes from e^+e^- annihilation, which provides very little sensitivity to the quark flavor dependence. Only a limited amount of charge-separated data from SIDIS and the BRAHMS experiment at RHIC is incorporated in the DSS FFs. The AKK FFs include charge-separated data for pions from BRAHMS and an earlier STAR measurement [31], but no SIDIS data. The DSS and AKK FFs include π^0 data from PHENIX and STAR, which improves constraints on gluon FFs to pions but does not provide sensitivity to quark flavor due to the zero isospin of the neutral pion. Furthermore, the SIDIS and e^+e^- data included in the fit are at a lower average fraction of the jet momentum (z) than the RHIC measurements, leading to weaker data-based constraints on the FFs in the z range most relevant to RHIC. The relevant z range covered by the present measurements is $\sim$ 0.45–0.71, determined by extracting the z distribution for the pQCD calculations shown in this paper for $5 < p_T < 13$ GeV/c using the DSS and AKK FFs independently. The calculations using the two FFs showed consistent results.

TABLE IV: Ratio of charged pion cross section, as shown in Fig. 6.

$\langle p_T \rangle$ (GeV/c)	Ratio	STAT	SYST
5.39	0.850	0.035	0.027
6.39	0.858	0.037	0.027
7.41	0.821	0.052	0.026
8.44	0.798	0.075	0.026
9.71	0.733	0.083	0.023
11.76	0.74	0.16	0.022

We note that a similar discrepancy exists between the calculated and measured η-to-π^0 ratio at midrapidity in p+p collisions [34, 59]. Both the η FFs [38] and π^0 FFs [35] included PHENIX data in the fits, which helped to constrain the fragmentation from gluons in particular. However, with the η and pion FF parameterizations performed independently, the correlation of the normalization uncertainty on the PHENIX pion and η cross sections was not taken into account, and the normalization was scaled within the uncertainty in opposite directions for the two measurements to minimize the χ^2 when the fits were performed along with other world data. We propose that future FF parameterizations include direct fits of particle production ratios in cases where data are available. We expect that fitting ratios directly could significantly improve constraints on FFs because of cancellations in systematic uncertainties both in the measured data and in the calculations. Improved knowledge of FFs can in turn improve extractions of helicity PDFs as well as other nonperturbative functions related to hadron structure.

B. Helicity Asymmetries

In Fig. 7, our charged pion A_{LL} results are compared with three different expectations based on different global analyses, or fits, of helicity PDFs to world polarized data. The Blümlein-Böttcher (BB) fit [60] and the de Florian, et al. (DSSV) fit [25] use a specified functional form to describe the helicity PDFs, while NNPDF [61, 62] use a neural network framework without a specified functional form, allowing for additional freedom in the fit. Both BB and NNPDF (version 1.0 of polarized NNPDF) used only polarized DIS data for their constraint; the DSSV fit also includes SIDIS data as well as RHIC data for π^0 and jet A_{LL}, which were found to significantly constrain Δg in the intermediate x range, 0.05–0.2. NNPDF recently released an updated helicity PDF fit to include RHIC jet and W boson data [27], but this new fit has not been used for the calculations shown in Fig. 7. The generally larger asymmetries predicted for positive pions than negative pions reflect a Δg that is positive in the fits that are used for these calculations. One must take care in directly comparing our data with these expectations, as the DSS FFs have been used to calculate the A_{LL} expectations. As discussed above, the accuracy of any FF when comparing positive to negative charged pions needs further study.

In Fig. 8, we compare our charged pion A_{LL} results with our previously published π^0 A_{LL} results. By comparing the ordering of the charged and neutral pions, one could get information on the sign of Δg independent of any FF assumptions. However, due to the lack of a dedicated hadron trigger in PHENIX, the statistical precision of the charged pion data is limited, and does not allow for clear sign determination with the current data. In future global analyses, the inclusion of these data should enhance sensitivity to the sign of the gluon polarization.

VI. SUMMARY

In summary, the invariant cross sections, ratio, and double-helicity asymmetries of charge-separated positive and negative pions produced at midrapidity in $\sqrt{s} = 200$ GeV p+p collisions have been measured. The p_T range of the cross section measurements is from 5–13 GeV/c; that of the asymmetries is from 5–12 GeV/c. The separate positive

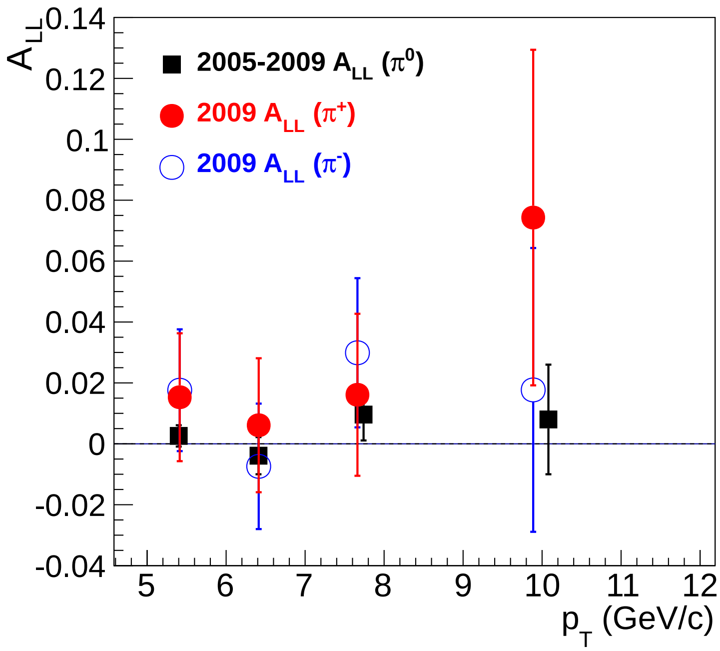

FIG. 8: (color online) Comparisons of double-helicity asymmetries for midrapidity positive, negative, and neutral pion production in p+p collisions at $\sqrt{s} = 200$ GeV measured by PHENIX. The neutral pion data are from [17].

and negative cross section measurements are consistent with NLO pQCD calculations within a large theoretical scale uncertainty and fall within $\sim \pm 20\%$ of the calculation at $\mu = p_T$ over the range presently measured. These charged pion cross section results, when included in FF fits, should improve predictions for future measurements. The NLO pQCD predictions for the ratio of negative to positive pion cross sections lie above the measurement by as much as 20%. This 20% difference does not fall within the range of ratios calculated using different choices of scale, the only uncertainty presently available on the ratio calculation, and indicates that other sources of systematic uncertainty on the ratio calculation need to be investigated. Inclusion of neutral pion data from RHIC in existing FF parameterizations has significantly improved constraints on the gluon-to-pion FF. Future FF fits which incorporate the present data, particularly the ratio data, will especially improve constraints on the flavor dependence of quark FFs to pions. To advance FF parameterizations more generally, we recommend that the phenomenology community move toward fitting measured particle ratios directly in cases where data are available because of the reduced uncertainties on both the measured and calculated quantities. In the future the charge-separated asymmetries with improved FFs in hand should be included in an updated global analysis of helicity PDFs. These data can increase sensitivity to the sign information of ΔG in future pQCD helicity PDF fits.

ACKNOWLEDGMENTS

We thank the staff of the Collider-Accelerator and Physics Departments at Brookhaven National Laboratory and the staff of the other PHENIX participating institutions for their vital contributions. We acknowledge support from the Office of Nuclear Physics in the Office of Science of the Department of Energy, the National Science Foundation, Abilene Christian University Research Council, Research Foundation of SUNY, and Dean of the College of Arts and Sciences, Vanderbilt University (U.S.A), Ministry of Education, Culture, Sports, Science, and Technology and the Japan Society for the Promotion of Science (Japan), Conselho Nacional de Desenvolvimento Científico e Tecnológico and Fundação de Amparo à Pesquisa do Estado de São Paulo (Brazil), Natural Science Foundation of China (P. R. China), Ministry of Education, Youth and Sports (Czech Republic), Centre National de la Recherche Scientifique, Commissariat à l'Énergie Atomique, and Institut National de Physique Nucléaire et de Physique des Particules (France), Bundesministerium für Bildung und Forschung, Deutscher Akademischer Austausch Dienst, and Alexander von Humboldt Stiftung (Germany), Hungarian National Science Fund, OTKA (Hungary), Department of Atomic Energy and Department of Science and Technology (India), Israel Science Foundation (Israel), Basic Science

Research Program through NRF of the Ministry of Education (Korea), Physics Department, Lahore University of Management Sciences (Pakistan), Ministry of Education and Science, Russian Academy of Sciences, Federal Agency of Atomic Energy (Russia), VR and Wallenberg Foundation (Sweden), the U.S. Civilian Research and Development Foundation for the Independent States of the Former Soviet Union, the Hungarian American Enterprise Scholarship Fund, and the US-Israel Binational Science Foundation.

---

[1] F. D. Aaron *et al.* (H1 and ZEUS Collaboration), J. High Energy Phys. **01** (2010) 109.
[2] R. J. Holt and C. D. Roberts, Rev. Mod. Phys. **82**, 2991 (2010).
[3] M. Burkardt, C. Miller, and W. Nowak, Rept. Prog. Phys. **73**, 016201 (2010).
[4] D. de Florian, R. Sassot, M. Stratmann, and W. Vogelsang, Prog. Part. Nucl. Phys. **67**, 251 (2012).
[5] C. A. Aidala, S. D. Bass, D. Hasch, and G. K. Mallot, Rev. Mod. Phys. **85**, 655 (2013).
[6] J. Ashman *et al.* (European Muon Collaboration), Phys. Lett. B **206**, 364 (1988).
[7] J. Ashman *et al.* (European Muon Collaboration), Nucl. Phys. B **328** (1989).
[8] B. Adeva *et al.* (Spin Muon Collaboration), Phys. Rev. D **58**, 112001 (1998).
[9] B. Adeva *et al.* (Spin Muon Collaboration), Phys. Rev. D **58**, 112002 (1998).
[10] K. Abe *et al.* (E143 collaboration), Phys. Rev. D **58**, 112003 (1998).
[11] J. R. Ellis and R. L. Jaffe, Phys. Rev. D **9**, 1444 (1974), erratum-ibid.D10.1669,1974.
[12] R. Jaffe and A. Manohar, Nucl. Phys. B **337**, 509 (1990).
[13] E. Leader and C. Lorce, Phys. Rept. (2013).
[14] M. Wakamatsu, Int. J. Mod. Phys. A **29**, 1430012 (2014).
[15] A. Adare *et al.* (PHENIX Collaboration), Phys. Rev. Lett. **103**, 012003 (2009).
[16] A. Adare *et al.* (PHENIX Collaboration), Phys. Rev. D **79**, 012003 (2009).
[17] A. Adare *et al.* (PHENIX Collaboration), Phys. Rev. D **90**, 012007 (2014).
[18] B. Abelev *et al.* (STAR Collaboration), Phys. Rev. Lett. **100**, 232003 (2008).
[19] L. Adamczyk *et al.* (STAR Collaboration), Phys. Rev. D **86**, 032006 (2012).
[20] L. Adamczyk *et al.* (STAR Collaboration), arXiv:1405.5134.
[21] A. Adare *et al.* (PHENIX Collaboration), Phys. Rev. Lett. **106**, 062001 (2011).
[22] M. Aggarwal *et al.* (STAR Collaboration), Phys. Rev. Lett. **106**, 062002 (2011).
[23] L. Adamczyk *et al.* (STAR Collaboration), Phys. Rev. Lett. **113**, 072301 (2014).
[24] D. de Florian, R. Sassot, M. Stratmann, and W. Vogelsang, Phys. Rev. Lett. **101**, 072001 (2008).
[25] D. de Florian, R. Sassot, M. Stratmann, and W. Vogelsang, Phys. Rev. D **80**, 034030 (2009).
[26] E. Aschenauer, A. Bazilevsky, K. Boyle, K. Eyser, R. Fatemi, *et al.* (2013), arXiv:1304.0079.
[27] E. R. Nocera, R. D. Ball, S. Forte, G. Ridolfi, and J. Rojo (NNPDF Collaboration) (2014), arXiv:1406.5539.
[28] D. de Florian, R. Sassot, M. Stratmann, and W. Vogelsang, Phys. Rev. Lett. **113**, 012001 (2014).
[29] S. Adler *et al.* (PHENIX Collaboration), Phys. Rev. Lett. **91**, 241803 (2003).
[30] B. Abelev *et al.* (STAR Collaboration), Phys. Rev. C **75**, 064901 (2007).
[31] J. Adams *et al.* (STAR Collaboration), Phys. Lett. B **637**, 161 (2006).
[32] J. Adams *et al.* (STAR Collaboration), Phys. Rev. Lett. **97**, 152302 (2006).
[33] I. Arsene *et al.* (BRAHMS Collaboration), Phys. Rev. Lett. **98**, 252001 (2007).
[34] A. Adare *et al.* (PHENIX Collaboration), Phys. Rev. D **83**, 032001 (2011).
[35] D. de Florian, R. Sassot, and M. Stratmann, Phys. Rev. D **75**, 114010 (2007).
[36] D. de Florian, R. Sassot, and M. Stratmann, Phys. Rev. D **76**, 074033 (2007).
[37] S. Albino, B. Kniehl, and G. Kramer, Nucl. Phys. B **803**, 42 (2008).
[38] C. A. Aidala, F. Ellinghaus, R. Sassot, J. P. Seele, and M. Stratmann, Phys. Rev. D **83**, 034002 (2011).
[39] M. Epele, R. Llubaroff, R. Sassot, and M. Stratmann, Phys. Rev. D **86**, 074028 (2012).
[40] A. Adare *et al.* (PHENIX Collaboration), Phys. Rev. D **82**, 072001 (2010).
[41] S. Albino, Rev. Mod. Phys. **82**, 2489 (2010).
[42] A. Adare *et al.* (PHENIX Collaboration), Phys. Rev. D **87**, 012011 (2013).
[43] M. Allen *et al.* (PHENIX Collaboration), Nucl. Instrum. Methods Phys. Res., Sect. A **499**, 549 (2003).
[44] A. Adare *et al.* (PHENIX Collaboration), Phys. Rev. D **88**, 032006 (2013).
[45] S. Aronson *et al.* (PHENIX Collaboration), Nucl. Instrum. Methods Phys. Res., Sect. A **499**, 480 (2003).
[46] K. Adcox *et al.* (PHENIX Collaboration), Nucl. Instrum. Methods Phys. Res., Sect. A **499**, 489 (2003).
[47] L. Aphecetche *et al.* (PHENIX Collaboration), Nucl. Instrum. Methods Phys. Res., Sect. A **499**, 521 (2003).
[48] M. Aizawa *et al.* (PHENIX Collaboration), Nucl. Instrum. Methods Phys. Res., Sect. A **499**, 508 (2003).
[49] W. Anderson, B. Azmoun, A. Cherlin, C. Chi, Z. Citron, *et al.*, Nucl. Instrum. Methods Phys. Res., Sect. A **646**, 35 (2011).
[50] A. Hocker and V. Kartvelishvili, Nucl. Instrum. Methods Phys. Res., Sect. A **372**, 469 (1996).
[51] A. Adare *et al.* (PHENIX Collaboration), Phys. Rev. C **83**, 064903 (2011).
[52] G. Agakishiev *et al.* (STAR Collaboration), Phys. Rev. Lett. **108**, 072302 (2012).
[53] A. Adare *et al.* (PHENIX Collaboration), Phys. Rev. D **76**, 051106 (2007).

[54] M. Stratmann, private communication.
[55] B. Abelev *et al.* (STAR Collaboration), Phys. Rev. Lett. **97**, 252001 (2006).
[56] W. Tung, H. Lai, A. Belyaev, J. Pumplin, D. Stump, *et al.*, J. High Energy Phys. **0702**, 053 (2007).
[57] D. Stump, J. Pumplin, R. Brock, D. Casey, J. Huston, *et al.*, Phys. Rev. D **65**, 014012 (2001).
[58] J. Pumplin, D. Stump, R. Brock, D. Casey, J. Huston, *et al.*, Phys. Rev. D **65**, 014013 (2001).
[59] B. Abelev *et al.* (ALICE Collaboration), Phys. Lett. B **717**, 162 (2012).
[60] J. Blumlein and H. Bottcher, Nucl. Phys. B **841**, 205 (2010).
[61] R. D. Ball *et al.* (NNPDF Collaboration), Nucl. Phys. B **874**, 36 (2013).
[62] R. D. Ball, V. Bertone, S. Carrazza, C. S. Deans, L. Del Debbio, *et al.*, Nucl. Phys. B **867**, 244 (2013).